Ionization behavior of molecular hydrogen in intense laser fields: Influence of molecular vibration and alignment

Johann Förster, Yulian V. Vanne, and Alejandro Saenz
AG Moderne Optik, Institut für Physik, Humboldt-Universität zu Berlin, Newtonstraße 15, D-12489 Berlin, Germany
(Received 8 September 2014; published 20 November 2014)

The alignment- and internuclear-distance-dependent ionization of H_2 exposed to intense, ultrashort laser fields is studied by solving the time-dependent two-electron Schrödinger equation. In the regime of perturbative few-photon ionization, a strong dependence of the ionization yield on the internuclear distance is found. While this finding confirms a previously reported breakdown of the fixed-nuclei approximation for parallel alignment, a simpler explanation is provided and it is demonstrated that this breakdown is not due to vibrational dynamics during the laser pulse. The persistence of this effect even for randomly aligned molecules is demonstrated. Furthermore, the transition from the multiphoton to the quasistatic (tunneling) regime is investigated considering intense 800 nm laser pulses. While the obtained ionization yields differ significantly from the prediction of Ammosov-Delone-Krainov rates, we find a surprisingly good quantitative agreement after introducing a simple frequency-dependent correction to the standard tunneling formula.

DOI: 10.1103/PhysRevA.90.053424 PACS number(s): 32.80.Rm, 33.80.Rv

I. INTRODUCTION

The rapid development of intense, ultrashort laser pulses during the past decade offers the prospects to measure and manipulate molecules on their natural time scales (few femtoseconds to attoseconds). By investigating the response of small molecules to these laser fields, concepts to produce a real-time movie of the electronic and nuclear dynamics triggered in these molecules have been developed. The high-harmonic radiation emitted from these molecules contains information which may be used for, e.g., orbital tomography [1], probing of nuclear dynamics with sub-fs resolution [2–6], and following coupled electron-nuclear dynamics with time-resolved high-harmonic spectroscopy [7,8]. Notably, already the electrons emitted by ionization (seen as the first step of high-harmonic generation) contain structural information suitable for orbital imaging [9,10]. Moreover, a process termed Lochfraß allows us to create nuclear wave packets in neutral molecules and to measure them with sub-femtosecond and sub-angstrom resolution, adopting a pump-probe scheme [11–13].

In view of the many promising proposals, a deeper understanding of the molecular response to intense, ultrashort laser fields is desirable. Compared to atoms, the nuclear degrees of freedom (vibration and rotation) as well as the multicentered (nonspherically symmetric) electronic structure of molecules increase the complexity regarding their theoretical treatment. Thus, even molecular hydrogen H_2, despite being the simplest neutral molecule, remains a great challenge for theory when exposed to intense laser fields. This is especially true if the correlated two-electron Schrödinger equation is solved in all six dimensions. In the case of large laser frequencies, low intensities, and not too extremely short laser-pulse durations, lowest-order perturbation theory (LOPT) may be used. Thus, at first, perturbative one-photon ionization [14] (and references therein) and later on two- to four-photon ionization [15] of H_2 have been studied.

The direct numerical solution of the time-dependent Schrödinger equation (TDSE) describing H_2 in intense laser fields for fixed nuclei and a parallel alignment was first realized on a sophisticated grid [16] and then using a configuration-interaction expansion built from H_2^+ orbitals expressed in prolate spheroidal coordinates [17]. In the perturbative regime, good quantitative agreement between LOPT and TDSE ionization yields has been found [17]. This latter approach has also been applied, e.g., for longer wavelengths and higher intensities as well as for nonparallel orientations of the laser polarization with respect to the molecular axis [18–21]. It was shown in [21] that a simplified treatment using the molecular strong-field approximation (in velocity gauge) can contradict the behavior obtained from the direct TDSE solution even qualitatively.

In a different approach based on an expansion in Born-Oppenheimer eigenstates and a single-center expansion for the electronic problem, the TDSE has been solved accounting also for vibrational dynamics [22] (neglecting nonadiabatic couplings). Large differences between the treatment that included the vibrational dynamics and the fixed-nuclei approximation were found [22–24]. Later applications of this approach concentrated mainly on low laser intensities and studied, e.g., the decay of autoionizing states [25,26]. Another, more recently introduced approach, again using prolate spheroidal coordinates but Laguerre and Legendre polynomials as basis functions, has been applied to investigate enhanced ionization occurring at large internuclear distances [27].

In the following section, the method to solve the two-electron TDSE and the basis-set parameters used are briefly discussed. In Sec. III, the method is applied in the perturbative multiphoton regime and compared to the results in Refs. [22–24]. In particular, the breakdown of the widely used fixed-nuclei approximation is reinvestigated in detail with the present approach. Furthermore, the study is extended to nonparallel (random) orientations of the laser polarization with respect to the molecular axis. The internuclear-distance dependent ionization behavior in the transition from the multiphoton regime to the quasistatic regime is studied in Sec. IV for the widely adopted Ti:sapphire wavelength. A parallel as well as a perpendicular orientation of the laser polarization with respect to the molecular axis is considered. The ionization yield is compared to the one obtained from

the approximate Ammosov-Delone-Krainov (ADK) tunneling rates [28]. Returning to the original Perelomov-Popov-Terent'ev [29] theory, a correction to the ADK tunneling rate is introduced and compared to the TDSE results.

II. METHOD

The method to solve the TDSE describing molecular hydrogen exposed to a laser field within the fixed-nuclei approximation is discussed in detail in previous works [17,19,20]. Briefly, the TDSE

$$i\frac{\partial}{\partial t}\psi(\mathbf{r},t) = (\hat{\mathrm{H}}_0 + \hat{\mathrm{V}}(t))\psi(\mathbf{r},t) \tag{1}$$

is solved by expanding the time-dependent electronic wave function $\psi(\mathbf{r},t)$ in terms of eigenstates of the field-free electronic Hamiltonian $\hat{\mathrm{H}}_0$ ($\mathbf{r}$ represents the set of both electronic coordinates). The latter eigenstates are obtained from a configuration-interaction (CI) calculation in which the Slater determinants are formed with the aid of H_2^+ eigenstates expressed in terms of B splines in prolate spheroidal coordinates [30]. Unless noted otherwise, atomic units with $\hbar = e = m_e = 4\pi\epsilon_0 = 1$ are adopted in this work. The linearly polarized laser pulse is described classically by the vector potential

$$\vec{A}(t) = \begin{cases} \vec{A}_0 \cos^2(\pi t/T)\sin(\omega t + \varphi) & \text{for} \quad |t| \leqslant T/2, \\ 0 & \text{elsewhere,} \end{cases} \tag{2}$$

with laser frequency ω, total pulse duration $T = 2\pi n_c/\omega$ (number of cycles n_c), and carrier-envelope phase φ. The interaction potential reads $\hat{\mathrm{V}}(t) = \hat{\mathbf{p}}\cdot\vec{A}(t)$ (dipole approximation, velocity gauge). To obtain the ionization yield, the electronic problem is solved for a single fixed internuclear distance R and alignment angle θ. Here, $\theta = 0$ corresponds to a parallel alignment ($\parallel$) of the polarization direction with respect to the molecular axis and $\theta = \pi/2$ corresponds to a perpendicular alignment ($\perp$). The ionization yield $Y(R,\theta)$ is then given by the population of all electronic continuum states (i.e., all two-electron states with an energy above the first continuum threshold which corresponds to the H_2^+ ground state energy) after the laser pulse. The ionization yield (or ionization probability) is normalized such that for $Y = 1$ every molecule is (at least) singly ionized.

The main basis-set parameters adopted for the present calculations are discussed in detail in [20]. Briefly, a box size of about 350 a.u. with 350 B splines of order $k = 10$ were used along the ξ coordinate (knot distribution: geometric progression with $g = 1.05$ for the first 40 intervals and linear progression afterwards). 30 B splines of order 8 with a linear knot sequence were used along the η coordinate and highly oscillatory H_2^+ orbitals with more than 19 nodes along η were omitted in the CI calculation. The CI expansion consists of a very long configuration series where one electron occupies the H_2^+ ground-state $1\sigma_g$ while the other occupies one of the remaining (bound or discretized continuum) H_2^+ eigenstates. This configuration series is mainly responsible to describe ionization. Together with additional CI configurations which represent doubly excited situations (responsible for the description of correlation and doubly excited states), this corresponds to about 6000 configurations per symmetry. Obtaining sufficiently converged TDSE solutions is computationally much more challenging for the 800 nm laser pulses discussed in Sec. IV compared to the perturbative regime in Sec. III.

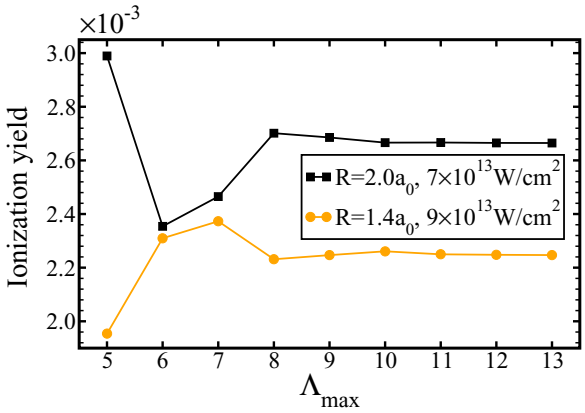

FIG. 1. (Color online) Convergence of the total ionization yield for a perpendicular-aligned H_2 molecule with respect to the maximal absolute value of the component of the total angular momentum along the internuclear axis, Λ_{max}, in a 20-cycle $\cos^2$-shaped 800 nm laser pulse.

For the results shown in Sec. III, states with energies up to 1 a.u. above the ionization threshold were included in the time propagation (0.5 a.u. are already sufficient). For nonparallel alignments, states with maximal absolute values of the component of the total angular momentum along the internuclear axis were included up to $\Lambda_{max} = 7$ (convergence was found already with $\Lambda_{max} = 4$). Furthermore, convergence with respect to the box size has been checked by doubling the box size. Most importantly, the CI expansion as described in [20] leads to a nonperfect description of the ground state of H_2, especially its energy. When comparing the multiphoton spectra obtained with the present method to methods that involve a practically correct ground-state energy (or possibly to future experimental ones), it is reasonable to correct for the error in the ground-state energy. As it was done in the perturbative study of H_2 in Ref. [15], a correction is obtained by shifting (or redefining) the laser frequency ω in the final graphs. Thus, a shifted frequency $\omega = \omega_{num} + \Delta\omega$ with $\Delta\omega = 0.0092$ a.u.[1] is used for our results shown in Sec. III (ω_{num} is the frequency used in the numerical calculation). It was found that this frequency shift $\Delta\omega$ is reduced when using a more complete CI expansion, but other than this shift no significant change in the ionization behavior was observed.

In the case of 800 nm (Sec. IV), states with energies up to 10 a.u. above the ionization threshold were included as in [20]. Furthermore, at this wavelength the treatment of the perpendicular alignment is much more challenging than the parallel one. Figure 1 shows the typical convergence of the total ionization yield with respect to Λ_{max} for two different intensities and internuclear distances. For the purpose of

[1]The shift $\Delta\omega = 0.0092$ a.u. corrects the energy difference between the $X^1\Sigma_g^+$ and $B^1\Sigma_u^+$ states and thus especially the resonance position of the $X^1\Sigma_g^+ \rightarrow B^1\Sigma_u^+$ transition at the equilibrium internuclear distance.

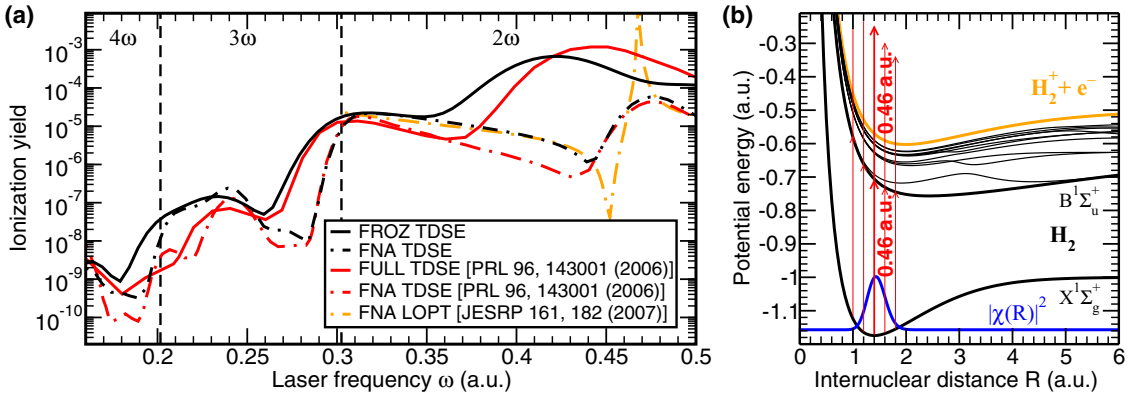

FIG. 2. (Color online) (a) Ionization yields as a function of the laser frequency ω for parallel-aligned H_2 exposed to $T = 10$ fs, $I = 10^{12}$ W cm^{-2} cos^2-shaped laser pulses. The dashed vertical lines indicate the borders between the two-, the three-, and the four-photon ionization regimes (2ω, 3ω, 4ω). The ionization yields obtained within the fixed-nuclei (FNA TDSE) and the frozen-nuclei (FROZ TDSE) approximations are compared to the perturbative fixed-nuclei (FNA LOPT) and the TDSE results fully including vibrational motion (FULL TDSE) extracted from Refs. [22–24]. (b) Potential-energy surfaces of H_2 (black lines), H_2^+ ionization threshold (orange/light grey line), and vibrational ground-state density $|\chi(R)|^2$ (blue or dark grey line). Furthermore, the resonant enhanced multiphoton ionization (REMPI) process $X^1\Sigma_g^+ \rightarrow B^1\Sigma_u^+ \rightarrow H_2^+(1\sigma_g) + e^-$ for different fixed internuclear separations is indicated by red (grey) vertical arrows.

this work, the values of $\Lambda_{\max} = 7$–11 were used to obtain sufficiently converged ionization yields, while higher values would be needed to obtain fully converged photoelectron spectra. A similar convergence behavior was observed with respect to the box size.

Within the *fixed-nuclei approximation* (FNA), the ionization yield $Y_{\rm FNA}(\theta) = Y(R_{\rm eq},\theta)$ is approximated by the electronic response at the equilibrium internuclear distance $R_{\rm eq} = 1.4$ a.u. While a treatment fully including vibrational dynamics (FULL) as in [22–24] is beyond the scope of the present paper, we may take nuclear vibration into account by "freezing" the initial nuclear wave function $\chi(R)$ (vibrational ground state of the electronic Born-Oppenheimer ground-state potential) during the time propagation. Within this *frozen-nuclei approximation* (FROZ),[2] the R-integrated ionization yield

$$Y_{\rm FROZ}(\theta) = \int dR\, Y(R,\theta)|\chi(R)|^2 \qquad (3)$$

is obtained from $Y(R,\theta)$ for a range of internuclear distances where the nuclear wave function $\chi(R)$ of the initial state is nonvanishing, namely $R = 1.0$–2.5 a.u. In Sec. III (IV), 61 (31) points separated by $\Delta R = 0.025$ a.u. (0.05 a.u.) were used. Furthermore, we consider different alignments of the laser polarization with respect to the molecular axis, especially also nonparallel ones ($\theta \neq 0$). In the case of a randomly aligned molecular ensemble, the alignment-averaged ionization yield

$$Y_{\rm avg,X} = \int_0^{\pi/2} d\theta\, \sin(\theta) Y_{\rm X}(\theta) \quad \text{with X = FNA or FROZ} \qquad (4)$$

is calculated from the fixed- or the frozen-nuclei ionization yields $Y_{\rm X}(\theta)$ obtained for various alignment angles θ. In the case of perturbative one-photon ionization, Eq. (4) can be simplified to $Y_{\rm avg}^{(1\omega)} = \frac{1}{3}Y_\parallel + \frac{2}{3}Y_\perp$. For the few- to many-photon ionization processes discussed here, however, the whole integration in Eq. (4) has to be performed. Thus, ten angles separated by $\Delta\theta = \pi/18$ were used in Sec. III. Clearly, nonparallel alignments are geometrically preferred over parallel ones due to the $\sin(\theta)$ factor. However, enhanced ionization of the formed H_2^+ ion at larger internuclear distances which occurs for a parallel alignment may obscure this fact in experiments.

[2]There exists no unified terminology for this level of approximation. It was termed frozen-nuclei limit in [37] and we use "frozen-nuclei approximation" throughout this paper.

III. PERTURBATIVE MULTIPHOTON REGIME

We study the ionization behavior for laser pulses in the perturbative multiphoton regime with a peak intensity of $I = 10^{12}$ W cm^{-2}, total duration $T = 10$ fs, carrier-envelope phase $\varphi = \pi/2$ and laser frequencies varying between $\omega = 0.16$ and 0.5 a.u. This allows us to directly compare the results obtained with the present method to those previously reported in [22–24].

Figure 2(a) shows the obtained ionization yields in direct comparison to the TDSE and LOPT results reported in [22–24] (parallel alignment, i.e. $\theta = 0$). We find a good qualitative and partly also quantitative agreement between our results and the FNA TDSE results reported in Refs. [22–24]. Furthermore, the agreement between our FNA TDSE ionization yields and the FNA LOPT yields for two-photon ionization obtained in [24] is very good. Differences between the TDSE and LOPT ionization yields are found only around $\omega \approx 0.46$ a.u. where the simple LOPT approach used in [24] diverges due to the resonant enhanced multiphoton ionization (REMPI) process $X^1\Sigma_g^+ \rightarrow B^1\Sigma_u^+ \rightarrow H_2^+(1\sigma_g) + e^-$ [see Fig. 2(b)]. In fact, a similarly good quantitative agreement between LOPT and TDSE ionization yields obtained with the present approach was found already earlier for one-, two-, three-, and four-photon ionization of H_2 (pulse parameters $T = 15$ fs, $I = 2 \times 10^{12}$ W cm^{-2}); see Fig. 3 in Ref. [17].

Although vibrational dynamics on a timescale of the order of 10 fs is expected to affect the ionization behavior and

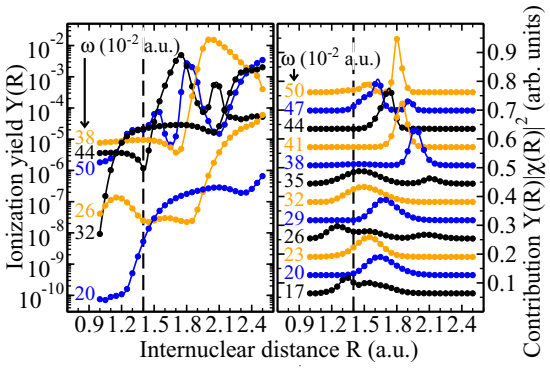

FIG. 3. (Color online) Ionization of parallel-aligned H_2 for $T = 10$ fs, $I = 10^{12}$ W cm^{-2} cos^2-shaped laser pulses and different laser frequencies ω. The left panel shows the fixed-nuclei ionization yields $Y(R)$ as a function of the internuclear distance R, whereas the right panel displays the contribution $Y(R)|\chi(R)|^2$ to the frozen-nuclei ionization yield in Eq. (3) (for better visibility scaled and vertically shifted).

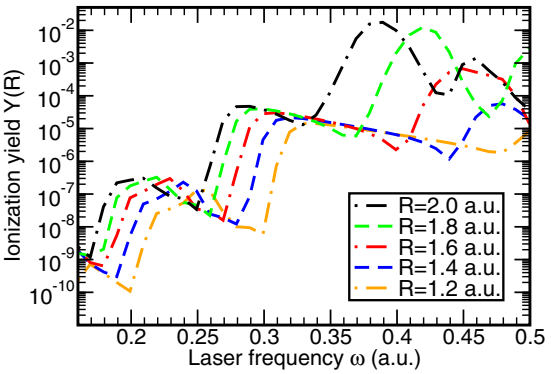

FIG. 4. (Color online) Fixed-nuclei ionization yields $Y(R)$ for parallel-aligned H_2 as a function of the laser frequency ω for different internuclear distances R. (Laser parameters as in Fig. 3.)

thus a perfect quantitative agreement between FROZ and FULL TDSEs is not expected, Fig. 2(a) shows that the ionization yield obtained within the FROZ TDSE behaves qualitatively surprisingly similar to the FULL TDSE results of Refs. [22–24]. When comparing the FROZ and FULL TDSEs ionization yields with their respective FNA results, both treatments show the same breakdown of the FNA, in particular a change of up to three orders of magnitude of the ionization yield around $\omega \approx 0.44$ a.u. Thus, already the rather simple FROZ treatment allows for an explanation of this preeminent breakdown of the FNA. Clearly, the ionization yield $Y(R)$ must strongly depend on the internuclear distance R in order to obtain an ionization yield significantly different compared to the FNA; see Eq. (3). At first glance, a strong dependence of the ionization yield on the internuclear distance R may not be expected since the transition dipoles do not dramatically depend on R in the vicinity of the equilibrium distance $R_{\rm eq} = 1.4$ a.u. (see, e.g., [23]). However, for REMPI, the energy differences between the electronic states determine where the resonance frequency or energy is located and thus play a crucial role. For molecules, these resonance frequencies depend significantly on the nuclear configuration. As an example, for the already mentioned REMPI process $X^1\Sigma_g^+ \rightarrow B^1\Sigma_u^+ \rightarrow H_2^+(1\sigma_g) + e^-$, Fig. 2(b) illustrates that at larger internuclear distances, $R > 1.4$ a.u., significantly lower laser frequencies, $\omega < 0.46$ a.u., are required to fulfill the resonance condition.

The dependence of the ionization yield $Y(R)$ on the internuclear distance R and the corresponding contribution $Y(R)|\chi(R)|^2$ of internuclear distances to the R-integrated ionization yield [Eq. (3)] is shown in Fig. 3. In general, the ionization yield $Y(R)$ changes many orders of magnitude with varying R. It might be surprising that for $\omega = 0.2$, 0.29, and $\geqslant 0.38$ a.u. the equilibrium distance $R_{\rm eq} = 1.4$ a.u. practically does not contribute at all to the total ionization yield. Of course, large differences between the FNA and FROZ or FULL treatments are observed for these frequencies in Fig. 2(a). In particular, for the breakdown of the FNA in the two-photon regime, i.e., for frequencies ω between 0.38 and 0.47 a.u., one can see how the R-integrated ionization yield is dominated by increasingly larger internuclear distances with lower and lower laser frequency. This is compatible with the expectation stemming from the simple picture in Fig. 2(b).

Figure 4 displays how the frequency dependence of the fixed-nuclei ionization yield $Y(R)$ changes with internuclear distance. For increasing internuclear distance, the threshold between N and $N+1$ photon ionization shifts to lower laser frequencies. Thus, while at the equilibrium distance $R_{\rm eq} = 1.4$ a.u. four-photon (three-photon) ionization occurs at the laser frequency $\omega = 0.2$ a.u. (0.29 a.u.), three-photon (two-photon) ionization occurs at larger internuclear distances. This leads to a significantly enhanced ionization yield at larger internuclear distances and thus pronounced differences between the fixed- and the frozen-nuclei ionization approximations (see also Figs. 2 and 3). Furthermore, Fig. 4 shows how the previously mentioned two-photon REMPI $X^1\Sigma_g^+ \rightarrow B^1\Sigma_u^+ \rightarrow H_2^+(1\sigma_g) + e^-$ requires lower and lower laser frequencies (and also strongly increases in magnitude) with increasing internuclear distance. The frequency shift of the ionization thresholds and resonance frequencies with internuclear distance can also be seen in the perturbative ionization cross sections in Figs. 1–3 of Ref. [15]. Similar to the comparison of LOPT and TDSE in Ref. [17], only the two-photon resonances are, however, clearly visible as peaks in the ionization yield when solving the TDSE for short (order of $T = 10$ fs) pulses. Notably, also the resonance due to the second autoionizing state with $^1\Sigma_g$ symmetry belonging to the Q(1) series, Q(1) $^1\Sigma_g(2)$, is visible at $R = 2$ a.u. and around $\omega = 0.47$ a.u. in Fig. 3 (as reported in Ref. [15]). Despite the fact that the nuclear probability density $|\chi(R \approx 2.0 \text{ a.u.})|^2$ is very small, this resonance still contributes noticeably to the total ionization yield; see the second hump for $\omega = 0.47$ a.u. in Fig. 3, right panel.

So far, only a parallel alignment of the laser polarization with respect to the molecular axis has been considered. However, an experiment with unaligned molecules (i.e., random alignment) can experimentally be more easily realized. Compared to a parallel alignment, a nonparallel alignment is computationally much more expensive. This is due to the broken cylindrical symmetry. In this case, not only electronic eigenstates with $^1\Sigma_g^+$ and $^1\Sigma_u^+$ symmetry, but considerably

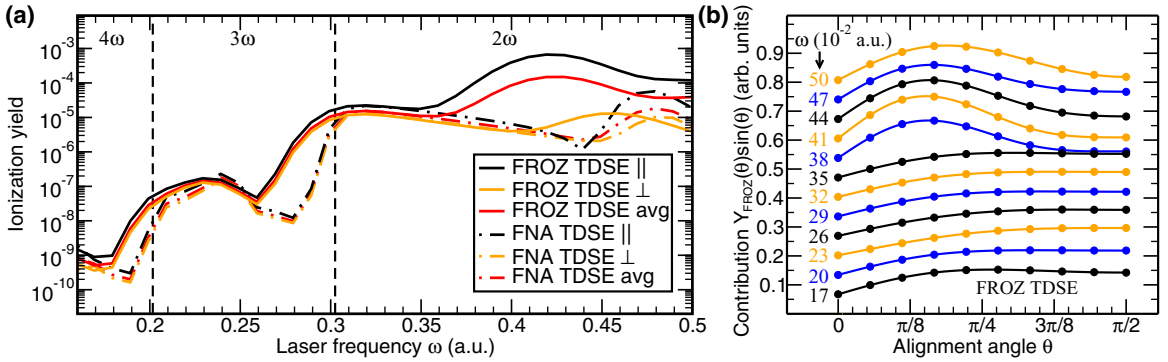

FIG. 5. (Color online) (a) Fixed- (FNA) and frozen-nuclei (FROZ) ionization yields as a function of the laser frequency ω for $T = 10$ fs, $I = 10^{12}$ W cm^{-2} cos^2-shaped laser pulses, and parallel ($\parallel$), perpendicular ($\perp$), and random (avg) alignments of the H_2 molecule. (b) Contribution $Y_{\mathrm{FROZ}}(\theta)\sin(\theta)$ to the alignment-averaged frozen-nuclei ionization yield in Eq. (4) (for better visibility scaled and vertically shifted).

more symmetries have to be taken into account. However, since a single FNA TDSE calculation for parallel alignment in the perturbative regime is nowadays extremely fast (order of one second), it is comparatively simple to extend the previous study and to include the full alignment dependence together with the R dependence.

Figure 5(a) shows the FNA and the FROZ TDSE ionization yields for a parallel, a perpendicular, and a random alignment. The FNA TDSE behavior is similar to the behavior of the perturbative cross sections reported in Ref. [15]. For both FNA and FROZ TDSEs, the ionization yield for a parallel alignment is almost always higher than for a perpendicular alignment, whereas the alignment-averaged result lies in between. The alignment dependence of the ionization yield is rather small in the three- and four-photon ionization regime. In contrast, the result for a perpendicular alignment differs strongly from the parallel one in the two-photon case, especially in the frozen-nuclei treatment. The contributions $Y_{\mathrm{FROZ}}(\theta)\sin(\theta)$ of different alignment angles θ to the alignment-averaged ionization yield, see Eq. (4), are shown in Fig. 5(b). In contrast to the R dependence (Fig. 3) the alignment dependence is very smooth and a large portion of possible alignment angles contributes to the total ionization. In the three- and four-photon regime where the θ dependence of $Y_{\mathrm{FROZ}}(\theta)$ is rather small, the geometrically preferred alignment angles $\theta \lesssim \frac{\pi}{2}$ contribute most due to the $\sin(\theta)$ factor. In the two-photon regime, this geometrical preference competes with a strong dependence of the ionization yield $Y_{\mathrm{FROZ}}(\theta)$ on θ that shows the opposite trend, i.e., ionization is strongly enhanced for a parallel alignment. In conclusion, intermediate alignment angles around $\theta \approx \frac{\pi}{8}$ contribute most. Despite this huge alignment dependence for two-photon ionization, the previously discussed breakdown of the FNA is clearly seen in Fig. 5(a) also for randomly aligned molecules.

IV. INTENSE 800 nm LASER PULSES

We investigate the ionization behavior of hydrogen molecules exposed to intense laser pulses with the ubiquitous Ti:sapphire wavelength of 800 nm. The response to frequency-doubled 400 nm laser pulses has been studied earlier [20]. First, 800 nm cos^2 laser pulses with $n_c = 20$ cycles (FWHM of about 20 fs), carrier-envelope phase $\varphi = 0$, and peak intensities I varying between 2×10^{13} to 1.3×10^{14} W/cm^2 are considered. For this range of laser intensities, the Keldysh parameter [31]

$$\gamma = \omega \frac{\sqrt{2I_p}}{F} \tag{5}$$

[with the electron binding energy $I_p(R = 1.4\ \text{a.u.})$ and peak laser electric field strength F] varies for molecular hydrogen between $\gamma = 0.67$ and 2.6. This corresponds to the transition between the quasistatic ($\gamma \ll 1$) and the multiphoton ($\gamma \gg 1$) regimes. The dependence of the ionization yield $Y(R)$ on the internuclear distance R and the corresponding contribution $Y(R)|\chi(R)|^2$ of internuclear distances to the R-integrated ionization yield [Eq. (3)] is shown in Fig. 6. One can see a significant increase of the ionization yield $Y(R)$ with internuclear distance R, for example about 4 orders of magnitude for the intensity of 2×10^{13} W/cm^2. The R dependence of $Y(R)$ is very smooth compared to laser parameters in the perturbative regime, Fig. 3, and notably smoother than in the case of 400 nm [20]. This behavior was already observed earlier for shorter 6-cycle 800 nm pulses in Ref. [18] and is expected from the quasistatic picture in which the ionization rate depends smoothly (exponentially) on the R-dependent binding energy $I_p(R)$ [32,33]. However, on top of this smooth behavior resonance structures can be observed.

When comparing the results for parallel and perpendicular alignments of the molecule, i.e., the left and the right panels of Fig. 6, differences occur in the resonance behavior, especially resonance positions are shifted. Overall, one observes that the ionization behavior is quite similar for both alignments, i.e., the alignment dependence of the ionization yield is not a large (orders of magnitude) effect. The lower panel of Fig. 6 shows that the main contribution $Y(R)|\chi(R)|^2$ to the R-integrated ionization yields is shifted to larger internuclear distances $R > 1.4$ a.u. due to the strong increase of $Y(R)$ with increasing R. Nevertheless, this effect is smaller than the previously discussed breakdown of the FNA for two-photon ionization in Fig. 3.

The ionization yields can be compared to those obtained using the Ammosov-Delone-Krainov (ADK) tunneling rates

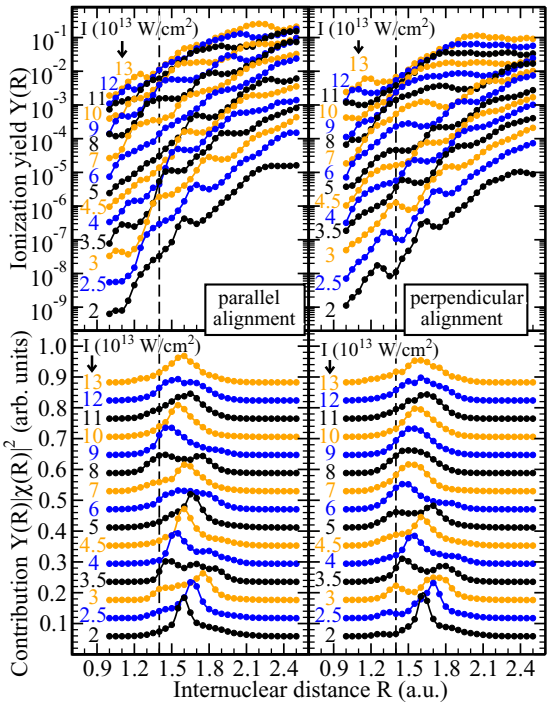

FIG. 6. (Color online) Ionization of H_2 molecules exposed to 20-cycle $\cos^2$-shaped 800 nm laser pulses and different laser peak intensities I. The upper panel shows the fixed-nuclei ionization yields $Y(R)$, whereas the lower panel displays the contribution $Y(R)|\chi(R)|^2$ to the frozen-nuclei ionization yield in Eq. (3) (scaled and vertically shifted). The left (right) panel shows the result for a parallel (perpendicular) alignment of the molecule with respect to the field axis.

Γ_{ADK} [28,34]. The ion yield

$$Y_{\mathrm{ADK}}(R) = 1 - \exp\left\{-\int \Gamma_{\mathrm{ADK}}[F_{\mathrm{e}}(t), I_p(R)]dt\right\} \quad (6)$$

is obtained by integrating the tunneling rate where $F_{\mathrm{e}}(t)$ is the envelope function of the electric field and the integration is performed over the whole pulse duration. For consistency, we use the vertical binding energy $I_p(R)$ obtained from the field-free CI calculation. Instead of using the envelope $F_{\mathrm{e}}(t)$ and the cycle-averaged ADK rate Γ_{ADK}, one may also perform the integral in Eq. (6) using the time-dependent electric field $F(t)$ and the static (instantaneous) rate $\sqrt{\pi\kappa^3/[3F(t)]}\Gamma_{\mathrm{ADK}}[F(t), I_p(R)]$. For the R-dependent ionization yields $Y_{\mathrm{ADK}}(R)$ shown in the following, the relative difference when using cycle-averaged or static rates remains below 1.3% and is thus negligible. Notably, in the transition regime studied here with $\gamma = 0.67$–2.6, the validity condition for the ADK rate, $\gamma \ll 1$, is not (strictly) fulfilled. The popular ADK rates differ from the Perelomov-Popov-Terent'ev (PPT) [29] rates by the restriction to the quasistatic regime $\gamma \ll 1$, the introduction of effective quantum numbers n^* and l^* for nonhydrogenic atoms (or molecules), an application of the Stirling approximation for the evaluation of factorials, and a rearrangement of the final expression. It is usually assumed that the pre-exponential factor in the ionization rate is less important than the exponential one. Returning to the original PPT theory [29], a simple correction to cycle-averaged ADK rates Γ_{ADK} is obtained by replacing the exponential

$$\exp\left[-\frac{2\kappa^3}{3F_{\mathrm{e}}}\right] \to \exp\left[-\frac{2\kappa^3}{3F_{\mathrm{e}}}\, g(\gamma)\right] \quad (7)$$

while leaving the prefactor unchanged. The function g is defined as [29]

$$g(\gamma) = \frac{3}{2\gamma}\left\{\left(1 + \frac{1}{2\gamma^2}\right)\mathrm{arcsinh}\gamma - \frac{\sqrt{1+\gamma^2}}{2\gamma}\right\} \quad (8)$$

with $\gamma = \kappa\omega/F_{\mathrm{e}}$ and $\kappa = \sqrt{2I_p(R)}$. Thus, starting from Eq. (7) in Ref. [34], one arrives at what we call "frequency-corrected ADK" (FC-ADK) rate

$$\Gamma_{\text{FC-ADK}} = N_e\sqrt{\frac{3F_{\mathrm{e}}}{\pi\kappa^3}(2/\kappa - 1)}\frac{F_{\mathrm{e}}}{8\pi}\left(\frac{4e\kappa^3}{(2/\kappa-1)F_{\mathrm{e}}}\right)^{2/\kappa} \times \exp\left[-\frac{2\kappa^3}{3F_{\mathrm{e}}}\, g(\gamma)\right] \quad (9)$$

where $e = 2.718\ldots$ and $N_e = 2$ is the number of active electrons. Notably, $g(\gamma)$ is a frequency-dependent modification to the standard ADK formula and the only ω-dependent term in Eq. (9). In the limit $\gamma \ll 1$ Eq. (9) reduces to the standard atomic ADK rate multiplied with the number of active electrons N_e.

Applying both ADK and FC-ADK models at the equilibrium internuclear distance leads to their predictions within the FNA, whereas the R integration similar to Eq. (3) results in the predictions within FROZ. Figure 7(a) shows the FNA and FROZ TDSE ionization yields for parallel and for perpendicular alignments compared to the ADK and FC-ADK results. For both fixed and frozen nuclei, one observes a rather small alignment dependence, i.e., the TDSE results for parallel and perpendicular alignments always agree within a factor of 3 (FNA) or 2 (FROZ) with a (mostly) slightly higher ionization yield for parallel alignment. Assuming that the alignment dependence relates to the symmetry of the initial state, this result is expected since the electronic ground state of H_2 is almost spherically symmetric. For the same reason, a simple one-electron one-center model potential [19,20,35] provides a good approximation for the ionization behavior of H_2. Most interestingly, while the ionization yields obtained with standard ADK differ from the TDSE results by several orders of magnitude, FC-ADK and TDSE ionization yields agree astonishingly well over the whole intensity range. The ratios $Y_{\mathrm{FROZ}}/Y_{\mathrm{FNA}}$ of the ionization yields in Fig. 7(a) are shown in Fig. 7(b). The ionization yield is significantly enhanced within the FROZ TDSE compared to the FNA, similar to the breakdown of the FNA for two-photon ionization in Fig. 2(a). Depending on the laser intensity (and alignment), this enhancement reaches almost one order of magnitude. The ADK and FC-ADK formulas predict a smooth increase of the ratio with decreasing intensity. While the overall behavior of the TDSE ratios agree well with the FC-ADK results, the TDSE ratios become more and more structured with decreasing intensity since resonance structures become more and more pronounced (see also Fig. 6). For example, at intensity $I = 4 \times 10^{13}$ W/cm^2, one finds $Y_{\mathrm{FROZ}}/Y_{\mathrm{FNA}} = 6.3$ (2.5) in the case of a parallel (perpendicular) alignment. At this laser intensity, a channel closing is expected such

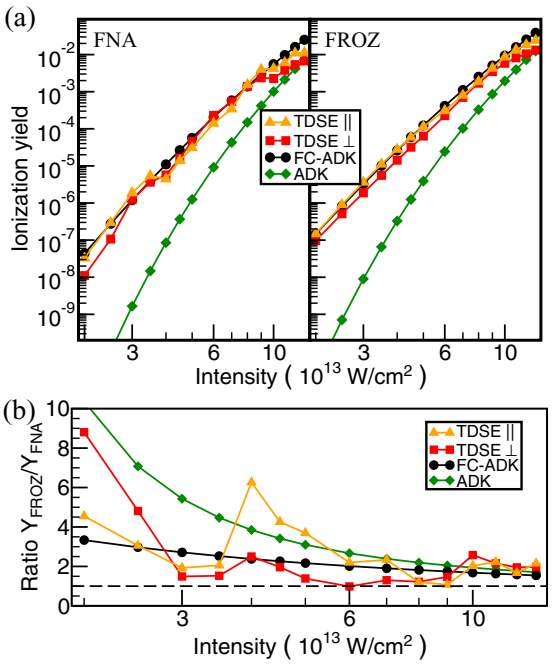

FIG. 7. (Color online) (a) Fixed- (FNA, left panel) and frozen-nuclei (FROZ, right panel) ionization yields of H_2 as a function of the peak intensity of a 20-cycle $\cos^2$-shaped 800 nm laser pulse for parallel and a perpendicular alignments of the molecule are compared with those predicted by the ADK model with (FC-ADK) and without (ADK) frequency correction. (b) Ratio $Y_{\mathrm{FROZ}}/Y_{\mathrm{FNA}}$ of the ionization yields shown in (a). The dashed horizontal line indicates $Y_{\mathrm{FROZ}}/Y_{\mathrm{FNA}} = 1$.

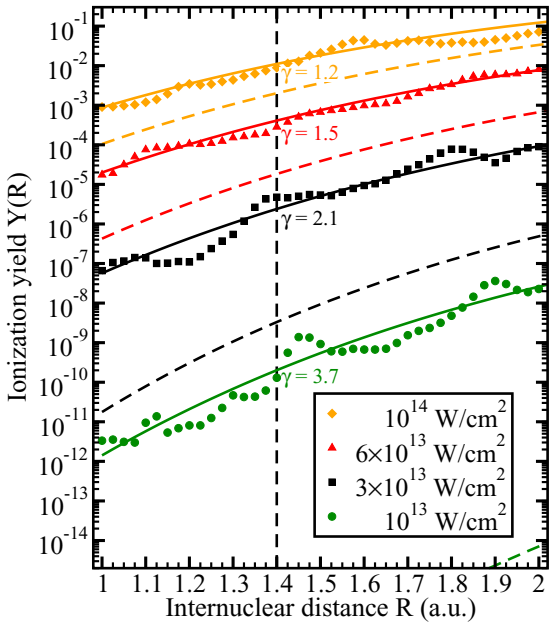

FIG. 8. (Color online) Ionization yields for a parallel-aligned H_2 molecule in 40-cycle $\cos^2$-shaped 800 nm laser pulses with different peak intensities are compared with those predicted using ADK (dash lines) and frequency-corrected ADK (solid lines) ionization rates. The corresponding Keldysh parameters γ are given inside the graph. The dashed vertical line indicates the equilibrium internuclear distance $R_{\mathrm{eq}} = 1.4$ a.u.

that 13 photons are required to overcome the ionization threshold at $R \leqslant 1.35$ a.u. while 12 photons are sufficient at $R > 1.35$ a.u. This leads to a strong increase of the ionization yield at internuclear distances which are slightly larger than the equilibrium distance (see Fig. 6) and thus to a strongly increased ionization yield after the integration over internuclear distances.

Figure 8 shows the R-dependent ionization yields for parallel-aligned H_2 exposed to 800 nm $\cos^2$ laser pulses with $n_c = 40$ cycles (FWHM of about 40 fs), carrier-envelope phase $\varphi = 0$, and peak intensities I between 10^{13} and 10^{14} W/cm^2. One observes that the R dependence becomes significantly smoother with increasing intensity, i.e., multiphoton resonances are, as expected, less and less pronounced when approaching the quasistatic regime. Comparing the TDSE ionization yields to standard ADK, one finds that ADK qualitatively predicts the correct R dependence of the ionization yield while it may differ quantitatively by several orders of magnitude. The quantitative agreement improves with increasing intensity, i.e., decreasing Keldysh parameter γ. In contrast to the standard ADK model, however, FC-ADK and TDSE ionization yields agree quantitatively surprisingly well for the whole intensity range. Of course, similar to the standard ADK model, the FC-ADK approach is not very suitable for extremely intense laser fields where, in the quasistatic length-gauge picture, over-the-barrier ionization is possible and tunneling formulas tend to overestimate the total ionization yield [33,36]. It was found already in Ref. [18] that it is possible to predict the R dependence of the TDSE ionization yield with the ADK formula even for $\gamma \gtrsim 1$, if the obtained yield $Y_{\mathrm{ADK}}(R)$ is multiplied with a constant prefactor. Considerably shorter 800 nm $\cos^2$ laser pulses with $n_c = 6$ cycles (FWHM of about 6 fs), carrier-envelope phase $\varphi = 0$, and peak intensities I between 3.5×10^{13} and 1.06×10^{14} W/cm^2 were investigated in Ref. [18]. The prefactors needed to match ADK to TDSE ionization yields range up to 75 for 3.5×10^{13} W/cm^2.[3] We recalculate the TDSE ionization yields for these laser pulses in order to compare them with the ADK model and especially the FC-ADK model introduced here with a higher R resolution. For fully converged results, the basis set as described in Sec. II is extended by a second (long) configuration series where one electron occupies the H_2^+ exited state $1\sigma_u$ while the other occupies one of the remaining (bound or discretized continuum) H_2^+ eigenstates. The resulting TDSE ionization yields are in good agreement with Ref. [18]. The R-dependent ionization yields for parallel-aligned H_2 exposed to these $n_c = 6$ cycle pulses are shown in Fig. 9. Compared to $n_c = 40$ cycle pulses (Fig. 8), resonances are much less pronounced since a shorter pulse is broader in the frequency domain. When compared to the TDSE, the FC-ADK model again

[3]Unfortunately, as it turns out the ADK rate in [18] had an additional prefactor $\sqrt{\pi\kappa^3/(3F)}$, i.e., $\sqrt{\pi\kappa^3/(3F)}\Gamma_{\mathrm{ADK}}$ was used instead of Γ_{ADK}. Thus, the more appropriate scaling factors for obtaining agreement between ADK and TDSE results in [18] are 75, 14, 5, and 2.5 for the laser peak intensities 3.5, 5.4, 7.8, and 10.6×10^{13} W/cm^{-2}, respectively.

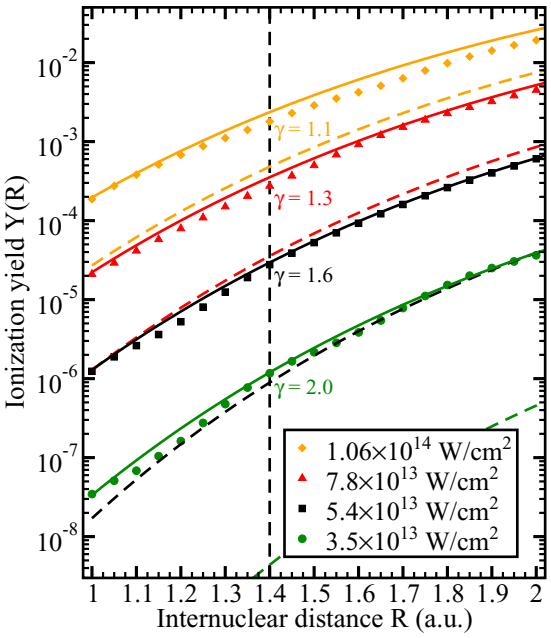

FIG. 9. (Color online) As Fig. 8, but for six-cycle pulses and other laser peak intensities.

predicts the correct R dependence almost quantitatively. Large scaling factors as required to match the behavior of ADK ionization yields to the TDSE results are thus not required for the FC-ADK model.

Despite the intrinsic shortcoming of the FC-ADK model to describe resonances, the excellent agreement between the TDSE and the FC-ADK model in the transition from the quasistatic to the multiphoton regime confirms the usefulness of the FC-ADK rates from Eq. (9), as shown for a range of laser intensities and pulse durations in Figs. 7–9.

V. CONCLUSIONS

The ionization behavior of molecular hydrogen exposed to high-frequency, low-intensity, as well as intense low-frequency (800 nm) laser pulses has been studied theoretically by solving the full-dimensional time-dependent two-electron Schrödinger equation. In the perturbative multiphoton ionization regime a good agreement between our TDSE results and TDSE as well as LOPT results reported in literature was found. Furthermore, a surprisingly strong dependence of the fixed-nuclei ionization yields $Y(R)$ on the internuclear distance R was found. This effect, caused by REMPI, offers a new explanation for the previously reported breakdown of the fixed-nuclei approximation for two-photon ionization [22–24]. The explanation, based on the frozen-nuclei approximation, still neglects vibrational dynamics during the laser field and considers only the initial spread of the nuclear wave function $\chi(R)$ in the initial state. Thus, this effect is expected to be important also for heavier molecules even though the actual laser-induced vibrational dynamics may be negligible. Notably, the frozen-nuclei approximation is computationally much simpler than the fully coherent treatment of electronic and nuclear motion and it provides a very simple picture for the interpretation of results (vertical transitions between electronic Born-Oppenheimer potentials). The alignment-dependence of the ionization yield turns out to be rather small for three- and four-photon ionization. In contrast, it is very pronounced in the two-photon regime. Nevertheless, even for randomly aligned molecules, the breakdown of the fixed-nuclei approximation for two-photon ionization is clearly visible.

For intense 800 nm laser pulses in the transition between the multiphoton and the quasistatic regimes, we found a comparably small alignment dependence. On the other hand, we observed a pronounced increase of the fixed-nuclei ionization yield $Y(R)$ with increasing internuclear distance R. This increase is well understood by the exponential dependence of the quasistatic ionization rate on the binding energy $I_p(R)$. The smooth R dependence is superimposed by multiphoton resonances which become less and less pronounced when approaching the quasistatic regime. We found that while the ADK formula qualitatively describes the increase of $Y(R)$ with R, it completely fails quantitatively for $\gamma \gtrsim 1$ (which is outside the validity region of the ADK model, $\gamma \ll 1$). Thus, motivated by the original PPT theory, the FC-ADK formula was introduced as a simple modification of the standard ADK formula. The quantitative agreement between the FC-ADK and the TDSE results for H_2 is astonishing and manifests the usefulness of the modified ADK formula. It may be even useful if no TDSE solution is available as for systems more complex than H_2, e.g., for the calibration of the laser intensity in experiments.

ACKNOWLEDGMENTS

The authors gratefully acknowledge financial support from the German National Academic Foundation (Studienstiftung des deutschen Volkes), the Humboldt Center for Modern Optics, the Fonds der Chemischen Industrie, the EU Initial Training Network (ITN) CORINF, and the European COST Action CM1204 (XLIC). This research was supported in part by the National Science Foundation under Grant No. PHY11-25915.

[1] J. Itatani, J. Levesque, D. Zeidler, H. Niikura, H. Pépin, J. C. Kieffer, P. B. Corkum, and D. M. Villeneuve, Nature (London) **432**, 867 (2004).

[2] M. Lein, Phys. Rev. Lett. **94**, 053004 (2005).

[3] S. Baker, J. S. Robinson, C. A. Haworth, H. Teng, R. A. Smith, C. C. Chirilă, M. Lein, J. W. G. Tisch, and J. P. Marangos, Science **312**, 424 (2006).

[4] J. P. Farrell, S. Petretti, J. Förster, B. K. McFarland, L. S. Spector, Y. V. Vanne, P. Decleva, P. H. Bucksbaum, A. Saenz, and M. Gühr, Phys. Rev. Lett. **107**, 083001 (2011).

[5] P. M. Kraus and H. J. Wörner, ChemPhysChem **14**, 1445 (2013).

[6] J. Förster and A. Saenz, ChemPhysChem **14**, 1438 (2013).

[7] H. J. Wörner, J. B. Bertrand, D. V. Kartashov, P. B. Corkum, and D. M. Villeneuve, Nature (London) **466**, 604 (2010).
[8] H. J. Wörner, J. B. Bertrand, B. Fabre, J. Higuet, H. Ruf, A. Dubrouil, S. Patchkovskii, M. Spanner, Y. Mairesse, V. Blanchet *et al.*, Science **334**, 208 (2011).
[9] M. Meckel, D. Comtois, D. Zeidler, A. Staudte, D. Pavičić, H. C. Bandulet, H. Pépin, J. C. Kieffer, R. Dörner, D. M. Villeneuve *et al.*, Science **320**, 1478 (2008).
[10] S. Petretti, Y. V. Vanne, A. Saenz, A. Castro, and P. Decleva, Phys. Rev. Lett. **104**, 223001 (2010).
[11] E. Goll, G. Wunner, and A. Saenz, Phys. Rev. Lett. **97**, 103003 (2006).
[12] T. Ergler, B. Feuerstein, A. Rudenko, K. Zrost, C. D. Schröter, R. Moshammer, and J. Ullrich, Phys. Rev. Lett. **97**, 103004 (2006).
[13] L. Fang and G. N. Gibson, Phys. Rev. Lett. **100**, 103003 (2008).
[14] F. Martín, J. Phys. B **32**, R197 (1999).
[15] A. Apalategui and A. Saenz, J. Phys. B **35**, 1909 (2002).
[16] K. Harumiya, I. Kawata, H. Kono, and Y. Fujimura, J. Chem. Phys. **113**, 8953 (2000).
[17] M. Awasthi, Y. V. Vanne, and A. Saenz, J. Phys. B **38**, 3973 (2005).
[18] M. Awasthi and A. Saenz, J. Phys. B **39**, S389 (2006).
[19] Y. V. Vanne and A. Saenz, J. Mod. Opt. **55**, 2665 (2008).
[20] Y. V. Vanne and A. Saenz, Phys. Rev. A **80**, 053422 (2009).
[21] Y. V. Vanne and A. Saenz, Phys. Rev. A **82**, 011403 (2010).
[22] A. Palacios, H. Bachau, and F. Martín, Phys. Rev. Lett. **96**, 143001 (2006).
[23] A. Palacios, H. Bachau, and F. Martín, Phys. Rev. A **75**, 013408 (2007).
[24] J. L. Sanz-Vicario, A. Palacios, J. C. Cardona, H. Bachau, and F. Martín, J. Electron Spectrosc. Relat. Phenom. **161**, 182 (2007).
[25] P. Rivière, R. E. F. Silva, and F. Martín, J. Phys. Chem. A **116**, 11304 (2012).
[26] R. E. F. Silva, P. Rivière, and F. Martín, Phys. Rev. A **85**, 063414 (2012).
[27] E. Dehghanian, A. D. Bandrauk, and G. L. Kamta, Phys. Rev. A **81**, 061403 (2010).
[28] M. V. Ammosov, N. B. Delone, and V. P. Krainov, Sov. Phys. JETP **64**, 1191 (1986).
[29] A. M. Perelomov, V. S. Popov, and M. V. Terent'ev, Sov. Phys. JETP **23**, 924 (1966).
[30] Y. V. Vanne and A. Saenz, J. Phys. B **37**, 4101 (2004).
[31] L. V. Keldysh, Sov. Phys. JETP **20**, 1307 (1965).
[32] A. Saenz, J. Phys. B **33**, 4365 (2000).
[33] A. Saenz, Phys. Rev. A **66**, 063408 (2002).
[34] F. A. Ilkov, J. E. Decker, and S. L. Chin, J. Phys. B **25**, 4005 (1992).
[35] A. Lühr, Y. V. Vanne, and A. Saenz, Phys. Rev. A **78**, 042510 (2008).
[36] A. Scrinzi, M. Geissler, and T. Brabec, Phys. Rev. Lett. **83**, 706 (1999).
[37] A. Saenz, Phys. Rev. A **66**, 063407 (2002).